Journal of Hazardous Materials 197 (2011) 144–152

Contents lists available at SciVerse ScienceDirect

Journal of Hazardous Materials

journal homepage: www.elsevier.com/locate/jhazmat

Rule of Fe^0 nano-particles and biopolymer structures in kinds of the connected pairs to remove Acid Yellow 17 from aqueous solution: Simultaneous removal of dye in two paths and by four mechanisms

Roohan Rakhshaee*

Department of Applied Chemistry, Faculty of Science, Islamic Azad University, Rasht Branch, P.O. Box 41335-3516, Rasht, Iran

ARTICLE INFO

Article history:
Received 28 April 2011
Received in revised form 8 September 2011
Accepted 17 September 2011
Available online 1 October 2011

Keywords:
Acid yellow 17
Modified Fe^0 nano-particles
Extracted pectin
Cross-linked

ABSTRACT

In this study, cyclohexane 1,3,5-tericarboxylic acid (CHA) and β-isopropylglutaric acid (IPA) were used to obtain the cross-linked forms of the extracted pectin from orange skin (PO), viz. PO-CHA and PO-IPA. These agents were used to stabilize the synthesized Fe^0 nano-particles (Fe^0 NPs) viz. the preparation of Fe^0-PO, Fe^0-PO-CHA and Fe^0-PO-IPA, to compare their ability for the removal of Acid yellow 17 (AY 17) from aqueous solution. FT-IR spectra specified that bidentate bridging and monodentate interaction were the primary mechanisms for binding PO-CHA and PO-IPA molecules to Fe^0 NPs, respectively. The removal percent of AY 17 was determined 97.8, 92.8, 84.1, 79.6, 72.8, 61.5 and 45.6 by Fe^0-PO-CHA, Fe^0-PO-IPA, Fe^0-PO, PO-CHA, PO-IPA, PO and Fe^0 NPs, respectively, for the dye initial concentration of 200 ppm, at the optimized conditions. In these agents, Fe^0 nano-particles performed the reduction process of AY 17, while the organic polymers performed its adsorption process.

1. Introduction

The colors in wastewater usually have azo groups and aromatic structures which are harmful for human and ecosystem due to their toxicity and stability. They can also decrease the transparency of water and influence photosynthesis activity which hinders the microbial activities of submerged organisms [1–3]. At present the major techniques for treating dye wastewater are adsorption process and biological treatment [4]. Mittal et al. attended to adsorption process on waste materials to remove the hazardous dyes from waste waters. They used de-oiled soya as an agricultural waste material and bottom ash as a waste of power plants to remove methyl violet [5], fast green FCF [6], congo red [7], phenol red [8], carmoisine A [9], chrysoidine Y [10], metanil yellow [11], erythrosine [12], brilliant green [13], light green SF (yellowish) [14]. Also, they used electrochemical and adsorption techniques to remove yellow ME 7 GL from industrial effluent [15]. Hen feathers as a potential adsorbent were also used to remove a hazardous dye by Mittal [16].

The biological process is difficult to start up and control [17], but the sorption of various dyes onto peat [18] pith [19], wood [20], bagasse fly ash [21] and fungal biomass [22] have been studied. Pectin-rich biomass such as fruit wastes and macro algae can also remove dyes and heavy metals [23,24].

Nanotechnology, as the other new method, is quickly developing in water treatment. At the same time, magnetic nano-adsorbents are composed of magnetic cores and polymeric shells. Compared to the traditional adsorbents, they not only can be manipulated or recovered rapidly by an external magnetic field but also possess quite good performance owing to high efficient specific surface area and the absence of internal diffusion resistance [25–27].

Due to the smaller particle size, larger specific surface area, higher density of reactive surface sites and greater intrinsic reactivity of surface sites [28], nanoscale zerovalent iron (Fe^0 nano-particles (Fe^0 NPs)) has gained prominence for environmental remediation, especially for the remediation of contaminants that are susceptible to reductive transformation such as azo dyes [29,30], halogenated organics [31], high valent heavy metals [32] and toxic inorganic anions [33].

Agglomeration of magnetic metal nanoparticles takes place primarily through direct interparticle interactions such as Van der Waals forces and magnetic interactions [34]. Agglomeration reduces the specific surface area and the interfacial free energy, thereby diminishing particle reactivity. A stabilizer can enhance dispersion of nanoparticles through (a) electrostatic repulsion and (b) steric hindrance [33].

Extensive studies have been devoted to stabilizing non Fe^0 NPs. For instance, to prevent nanoscale iron oxides from agglomeration, various stabilizers have been found to be effective, including surfactants [35] and polymers [36]. Obviously, not all of these stabilizers are applicable to the Fe^0 NPs nanoparticles of interest. For

* Tel.: +98 131 4223152; fax: +98 131 4223621.
E-mail address: rakhshaei@iaurasht.ac.ir

0304-3894/$ – see front matter © 2011 Elsevier B.V. All rights reserved.
doi:10.1016/j.jhazmat.2011.09.067

example, thiols and carboxylic acids can be reduced by Fe^0 NPs, some polymers might not function properly in water [37], some stabilizers themselves are not environmentally benign, and others are cost-prohibitive.

Wang et al. used carboxymethyl cellulose-stabilized zero-valent iron nanoparticles to reduce hexavalent chromium [38]. Mallouk and co-workers employed carbon nanoparticles and poly(acrylic acid) (PAA) as "vehicles" for stabilizing and/or delivering Fe-based nanoparticles [39]. He et al. used sodium carboxymethyl cellulose (CMC) to stabilize Fe–Pd nanoparticles for enhanced transport and dechlorination of trichloroethylene in soil and groundwater [40].

Saleh et al. proposed a new type of sorptive nanoparticles prepared by modifying commercial ZVI nanoparticles with so-called "block copolymer shells" consisting of a hydrophobic inner shell and a hydrophilic outer shell for dechlorination of dense nonaqueous-phase liquids (DNAPLs) [41].

Pectin is an important polysaccharide constituent of plant cell walls [42]. Pectin, alone and or in a biomass, due to having functional groups such as carboxyl–carboxylate, can remove metal ions [43,44] and dyes [45,46]. In our previous work it was shown that the carboxyl and carboxylate groups of *Lemna minor*'s pectin have the main role to remove cations [47].

The present study was started with due attention to the separate role and ability of biosorbent's pectin as a biopolymer and nano-magnetic agents as the nano-particles to remove the pollutants such as dyes and metal ions. Pectin was extracted from orange skin as the main agent of the dye uptake and the surface of the synthesized Fe^0 nanoparticles was modified by pectin. These modified agents were used to prepare the cross-linked forms as a novel nano-bio-adsorbent to reach a higher removal efficiency of Acid yellow 17 (AY 17).

2. Materials and methods

2.1. Extraction of pectin from orange skin

The orange skin waste was collected from a factory of fruit juice. 50 g of orange skin sample was washed three times with 2 L deionised water for 30 min and then was air-dried in sun. Pectin was extracted according to other studies [42,48,49].

2.2. Preparation of Fe^0-PO

For stabilization of the Fe^0 iron nano-particles with pectin, the method of He et al. was used [40]. He et al. connected sodium carboxymethyl cellulose on the surface of the Fe^0 nanoparticles. This selection was done with due attention to the presence of the carboxylate groups as the binding agent in pectin similar to CMC.

The deionized water and the pectin solution were purged with purified N_2 for 30 min to remove dissolved oxygen before use. A stock solution of 0.20 M $FeSO_4{\cdot}7H_2O$ was prepared right before use and then was added to the pectin solution through a burette to yield the desired concentration of Fe and pectin. The total reaction volume was 500 mL and the concentrations of Fe and pectin were selected 0.2 and 0.7 g/L, respectively. The mixture was purged with N_2 for 30 min to complete the formation of the Fe-PO complex.

The Fe^{2+} ions were then reduced to Fe^0 by adding a certain amount of sodium borohydride (molar ratio of $BH_4^-/Fe^{2+} = 2.0$) to the mixture [40]. To ensure efficient use of the reducing agent BH_4^-, the reactor system was operated under inert conditions through continuous vacuuming. The flask was shaken by hand during the reaction and was then centrifuged [40]. The obtained product is shown as Fe^0-PO.

2.3. Preparation of Fe^0-PO-IPA and Fe^0-PO-CHA (cross linking process)

Cross-linking reactions of pectin were done according to two methods: (a) by adding one third of the obtained Fe^0-PO and 2 mL of 1.2 M (2.4 mmol) β-isopropylglutaric acid (IPA) solution (from Merck) into 120 mL of 2.0 wt% acetic acid solution at 40°C mixing it for 4 h; the obtained product is shown as Fe^0-PO-IPA, (b) by adding one third of the remained Fe^0-PO, 2 mL of 1.2 M (2.4 mmol) cyclohexane 1,3,5-tericarboxylic acid (CHA) (from Merck) and 1 mL of 98% H_2SO_4 into 200 mL of ethanol, with stirring and refluxing at 40 °C for 4 h. The obtained product of this step is shown as Fe^0-PO-CHA.

Fig. 1 shows the cross-linking reactions of pectin by CHA (left-hand) and IPA (right-hand). The more study about the samples of the cross-linked pectin was performed by FT-IR, SHIMADZU-8900.

2.4. Dye removal experiments

AY 17 ($C_{16}H_{10}Cl_2N_4Na_2O_7S_2$) stock solutions were prepared from the analytical grade from Merck in distilled water. A series of 1 L plastic bottles containing 200 mL of AY 17 solution (200 ppm) was prepared. The same amounts (2 g/L) of Fe^0 NPs, Extracted pectin, PO-IPA, PO-CHA, Fe^0-PO-IPA and Fe^0-PO-CHA were separately added into these bottles. The solution pH was adjusted 6.0 ± 0.1 for Fe^0 NPs and 3.0 ± 0.1 for others as the obtained optimum values. The bottles were mixed at 300 rpm and 25 ± 1 °C. At preselected time intervals, samples were withdrawn and centrifuged with 6500 rpm for 3 min. Then the samples were analyzed for the dye content (C_e) by spectrophotometer (JENWAY, Model 6405) in 402 nm as λ_{max} of AY 17.

3. Results and discussion

3.1. TEM, FT-IR and XRD studies

Fig. 2(A–D) show the TEM images of Fe^0 NPs (A), Fe^0-PO (B), Fe^0-PO-IPA (C) Fe^0-PO-CHA (D). Fig. 2A suggests that the particles without using the stabilizer did not appear as discrete nanoscale particles, rather, they formed much bulkier dendritic flocs with varying optical density. The size of some denser flocs could be much larger than 800–900 nm. Thus, the particles did not have a high surface area.

Wang et al. showed that the size of some denser flocs of Fe^0 nanoparticles without the stabilization by carboxymethyl cellulose were much larger than 1 μm but their sizes range was from 20 to 100 nm in diameter after the stabilization [38]. This type of aggregation could be attributed to the electrostatic forces between nanoscale particles and small particles, as well as their surface tension interactions [32]. As a result, a lower surface area is likely and a poorer reactivity is expected.

The diameter of Fe^0 NPs was not less than 10 nm and about 80% of them were between 30–45 nm. About 3% of these particles were about 50 nm in diameter, whereas the stabilized particles by stabilizers as discrete particles were not more than 45 nm.

Fig. 2(B–D) show the images of the stabilized nanoparticles by PO, PO-IPA and PO-CHA, viz. Fe^0-PO (B), Fe^0-PO-IPA (C) Fe^0-PO-CHA (D), respectively. As can be seen, the stabilization ability of these agents is as follows: PO < PO-IPA < PO-CHA. Because, about 41% of Fe^0- in Fe^0-PO had the size of 40 nm in diameter and the diameter of only 20% of them was less than 17 nm, whereas in Fe^0-PO-IPA, about 39% of Fe^0 had the size of about 15 nm and only 12% of them had the diameter size of about 30–40 nm. In Fe^0-PO-CHA, diameter of about 97% of Fe^0 NPs was less than 17 nm and the diameter of 3% of them was about 23 nm.

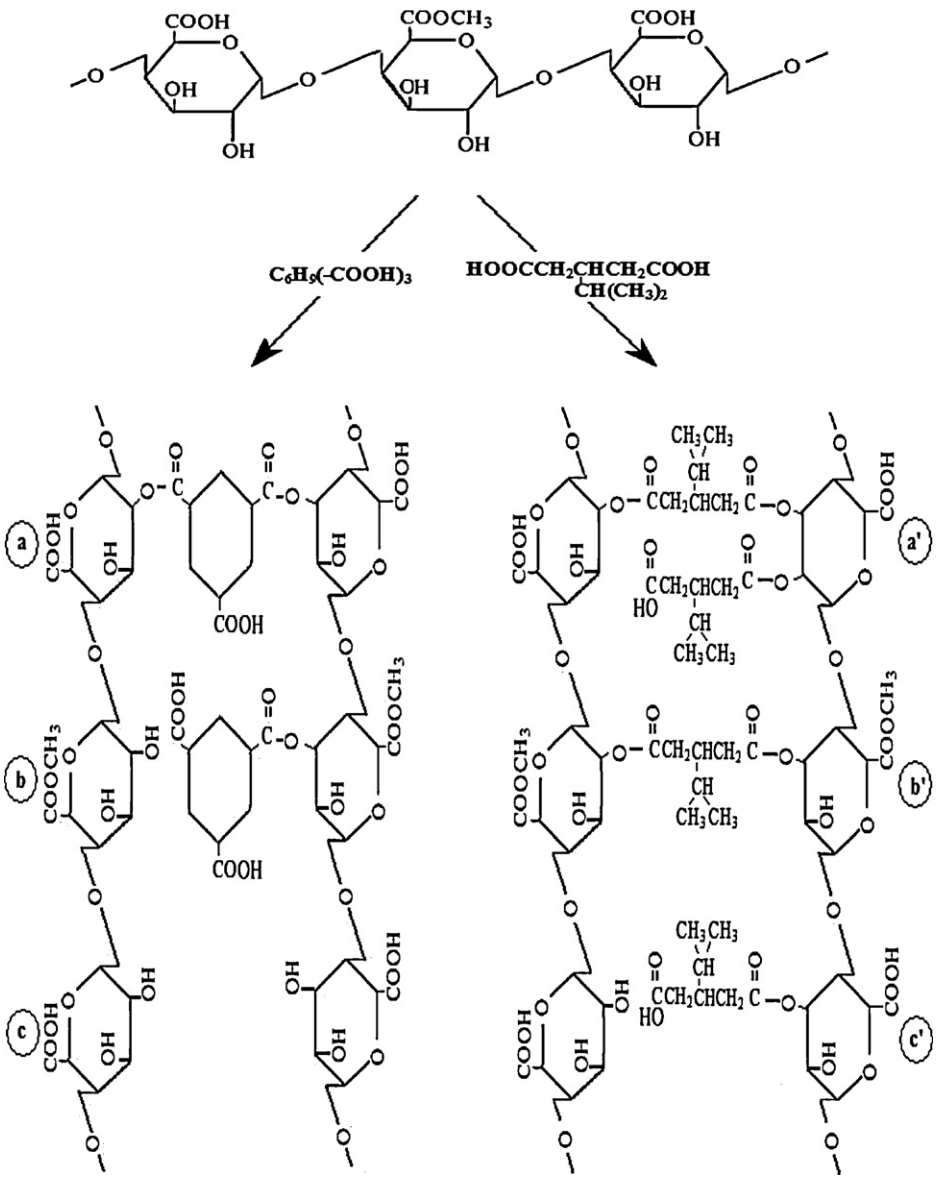

Fig. 1. Cross-linking reactions of pectin by CHA (left-hand) and IPA (right-hand).

Both the smaller mean size and the narrower distribution of Fe^0-PO-CHA indicate that PO-CHA better suppressed the growth of the iron nanoparticles and maintained a higher surface area of the particles.

Two main reason of the more suitable action of PO-CHA in comparison with PO-IPA can be as follows:

(1) the possibility and probability of having the more –COOH groups as a main agent of the connection to Fe^0 particles in the situation (b) of PO-CHA in comparison with (b′) of PO-IPA as 2:0, in despite of the fact that it is more in (c′) of PO-IPA in comparison with (c) of PO-CHA, because it is as 1:0 (see Fig. 1).
(2) the connection of each –COOH group of PO-CHA to two Fe^0 particles viz. bidentate bridging, in comparison with the connection each of them in PO-IPA to one Fe^0 particle, viz. monodentate interaction. Because, the separation of the symmetric and asymmetric stretches [$\Delta\upsilon = \Delta$ (asym) $- \Delta$ (sym)] of the carboxylate group can be used to determine the bonding mechanism when compared to that of the corresponding carboxylate salt [50,51]: If $\Delta = 200-320\,cm^{-1}$, the binding is governed by monodentate interaction; if $\Delta < 110\,cm^{-1}$, the binding is governed by bidentate chelating interaction; and if $\Delta = 140-190\,cm^{-1}$, the binding is governed by bidentate bridging (see Fig. 3). In our work, $\Delta\upsilon$ was $175\,cm^{-1}$ for Fe^0-PO-CHA and $207\,cm^{-1}$ for Fe^0-PO-IPA in FT-IR spectra (see Fig. 4).

Fig. 4 shows the FT-IR spectra of Fe^0-PO (A), Fe^0-PO-CHA (B) and Fe^0-PO-IPA (C). The broad and strong area of absorption between about 3600 and 2500 cm^{-1} in each spectra refers to O–H stretching absorption due to inter and intramolecular hydrogen bonds. This band at about $3500\,cm^{-1}$ for Fe^0-PO-CHA is broader and stronger than ones for Fe^0-PO-IPA. It could be due to the more presence probability of the alcoholic –OH groups in the situations (a), (b) and (c) as compared with the situations (a′), (b′) and (c′) in Fig. 1, so that the number ratio of the O–H groups according to probable and possible positions is as follows: (a′):(a) = 1:2, (b′):(b) = 2:3 and (c′):(c) = 3:4.

The mentioned band for Fe^0-PO-CHA has especially the more breadth at 2400–3320 cm^{-1} which could be due to the presence probability of the –OH groups of the excess –COOH from the non-reacted sites of Fe^0-PO-CHA in the situation (b) in Fig. 1 which

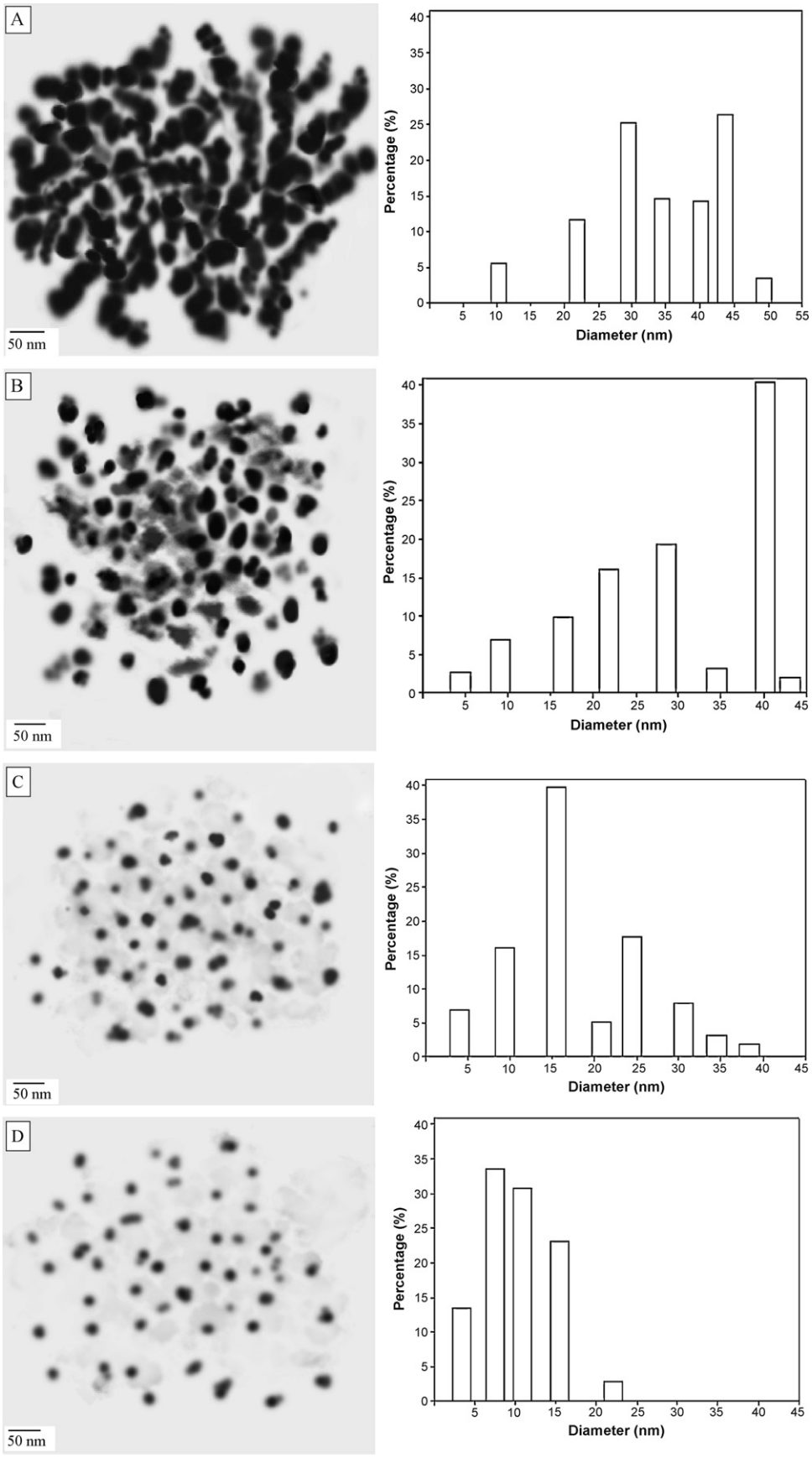

Fig. 2. TEM images of Fe^0 NPs (A), Fe^0-PO (B), Fe^0-PO-IPA (C) and Fe^0-PO-CHA (D).

is added to the alcoholic –OH stretching absorption of the pectin structure.

In the case of the esterified sites of pectin structure such as the situations (b) and (b′), an O–CH_3 stretching band would be expected between 2950 and 2750 cm^{-1} due to methyl esters of galacturonic acid. However, due to a large O–H stretching response occurring in a broad region, the O–CH_3 activity is masked and cannot a reliable indicator of methoxylation.

The peaks at 2925 cm^{-1} and 1720 cm^{-1} indicate C–H and C=O (ester carbonyl) absorption, respectively. The stronger peak at nearly 1720 cm^{-1} in the spectra of Fe^0-PO-IPA can be due to the more obtained strengthening C=O band (esterified) after the reaction between –COOH groups (from -PO-IPA) and –OH groups (from pectin) in the situations (a′) to (c′) in Fig. 1. Carboxylate (COO–) groups show two bands, an asymmetrical stretching band at 1642 cm^{-1}, and a weaker symmetric stretching band near 1435 cm^{-1}. These bands for Fe^0-PO-IPA are more intensive because these groups in this nano-bioparticles are more than those of Fe^0-PO-CHA.

As seen in Fig. 1, the ratio of the obtained C=O (esterified) according to probable and possible positions is as follows: (a′):(a) = 3:2, (b′):(b) = 2:1 and (c′):(c) = 1:0.

Furthermore, the absorption of C=O (carboxyl carbonyl) at 1700–1735 cm^{-1} due to the excess –COOH groups in the situations Fe^0-PO-CHA (in addition to –COOH of the pectin structure) is added and composed with the absorption of the carboxyl carbonyl, so they are seen as a stronger band in the spectra of Fe^0-PO-CHA. As seen in Fig. 1, the ratio of the obtained C=O (carboxyl carbonyl) according to probable and possible positions is as follows: (a′):(a) = 1:1, (b′):(b) = 0:2 and (c′):(c) = 1:0. The weak bands between 1200 and 1000 cm^{-1} correspond to the resonance absorption of pyranoid ring. The spectrum of Fe^0-PO (A) shows the peaks and characters of pectin's spectra.

Fig. 5 shows the XRD images of Fe^0-PO (A), Fe^0-PO-IPA (B) Fe^0-PO-CHA (C). The obtained peaks in the position and the relative intensity did not have obvious differences and all of them were for Fe^0 ($2\theta = 44.86^\circ$). So these results indicate that the modification of Fe^0 nanoparticles by pectin and cross-linked ones have not changed the crystal structure of nanoparticles, whereas the intensity of the peaks corresponding to the surface functional groups is reduced with using pectin and cross-linking agents. This reduction for Fe^0-PO-CHA is more than that of Fe^0-PO-IPA and Fe^0-PO. The crystal sizes of these agents were determined from the XRD pattern by using Scherrer's equation; $D = k\lambda/(\beta \cos\theta)$, where D is the average crystalline diameter, k is a constant (0.9 for Cu-kα), λ is X-ray wavelength (0.15405 nm for Cu-kα), β is the peak width of half-maximum of XRD diffraction lines and θ is Bragg's diffraction angle in degree. D values were obtained 19.5, 9.6 and 7.2 nm, respectively, which were similar to that observed from the TEM image.

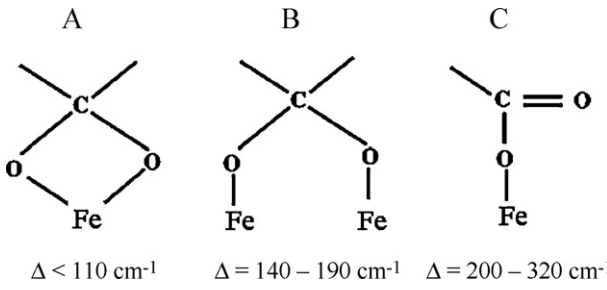

Fig. 3. Kinds of Fe^0-carboxylate complexation: (A) bidentate chelating, (B) bidentate bridging, and (C) monodentate chelating. Δ is the separation between the symmetric and asymmetric stretches of the carboxylate group.

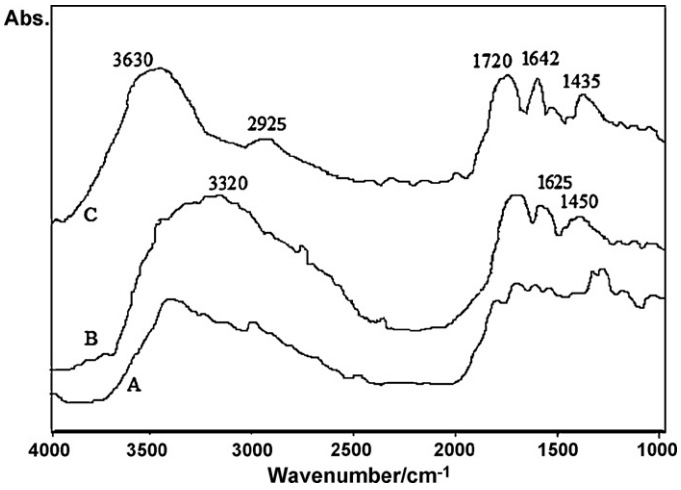

Fig. 4. FT-IR spectra of Fe^0-PO (A), Fe^0-PO-CHA (B) and Fe^0-PO-IPA (C).

3.2. Paths and mechanisms of AY 17 removal

The remover agents in this study can remove AY 17 in two overall paths. The first path is due to the performance of Fe^0 and the second path is due to acting the biopolymer structures. Therefore, Fe^0 NPs (without the stabilizers) in spite of the agglomeration, can use the first path, while PO, PO-IPA and PO-CHA use the second path, and Fe^0-PO, Fe^0-PO-IPA and Fe^0-PO-CHA use both paths.

Fe^0 particles in the first path use three mechanisms:

(1) Dye direct reduction, which is especially done at pH < 6, so Fe^0 and $(AY\ 17)^{2-}$ can be converted to Fe^{2+} and $(AY\ 17)^{4-}$ [52], (2) destroying the chromophore group and conjugated system of AY 17 as an azo dye, which can be performed by the generated atom H due to the reaction between Fe^0 and H_2O or H^+, that the iron corrosion and H^+ consumption lead to the increase of solution pH, (3) adsorption of dye on the Fe^0 products, which can be performed both on the intermediate products of Fe^0 and on the formed passive iron oxides layers.

On the one hand, the intermediate products of Fe^0 such as Fe^{2+}, Fe^{3+}, $Fe(OH)y^{2-y}$ (such as FeOH) are thermodynamically unstable and active [53]. Fe^{3+} can adsorb AY 17 and formed $[Fe(III)\text{-}(AY\ 17)]^+$ as a cationic complex at pH < 6. FeOH as a ferric hydroxide coated on the surface of Fe^0 can remove $(AY\ 17)^{2-}$ through the adsorption, at pH > 6 and is produced the anionic complex of $[FeOH\ (AY\ 17)]^-$ [52].

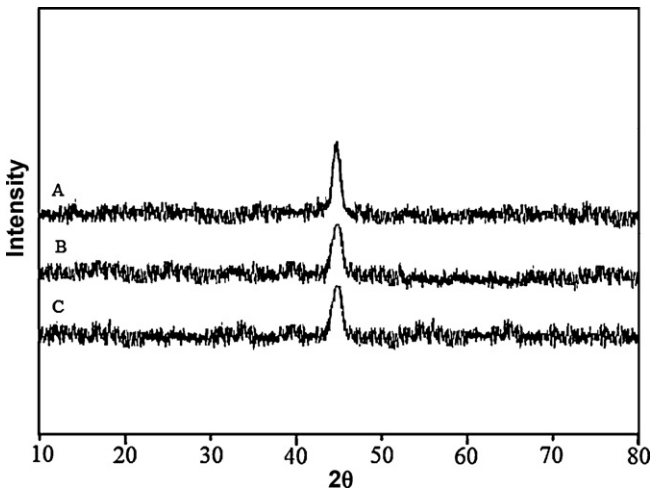

Fig. 5. XRD patterns of Fe^0-PO (A), Fe^0-PO-IPA (B) and Fe^0-PO-CHA (C).

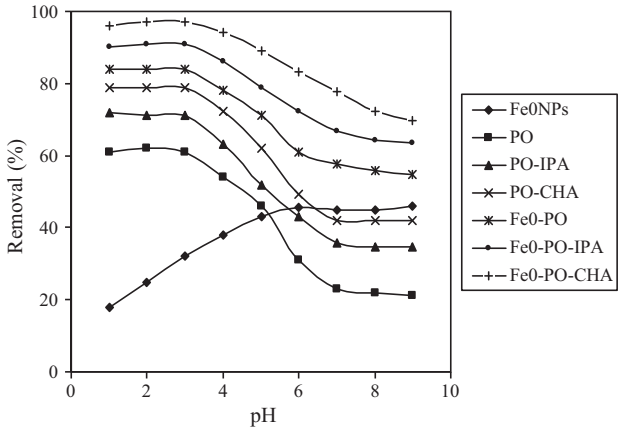

Fig. 6. Effect of initial solution pH on the AY 17 removal by the kinds of remover agents: initial concentration of AY 17: 200 ppm, remover agents dose: 2.0 g/L, contact time: 100 min, temperatures: 298 K, agitation rate: 300 rpm.

On the other hand, the formed passive iron oxides layers (Fe_3O_4, Fe_2O_3, $Fe(OH)_3$, and FeOOH) [54–56] can also adsorb dye molecules via the sulfonic group and reduce the dye through the formation of a bridged bidentate complex [57].

Biopolymer structures in the second path use one mechanism as the fourth mechanism. It is the adsorption of dye by –COOH and –OH groups of pectin and its cross-linked forms as the main mechanism. The carboxyl and hydroxyl groups are converted to $–COOH_2^+$ and $–OH_2^+$ at the acidic pHs, so an electrostatic attraction is happened between these positive groups and $–SO_3^-$ of the acidic dyes. Therefore PO, PO-IPA, PO-CHA and the pectin structure in Fe^0-PO-IPA and Fe^0-PO-CHA can use this mechanism to absorb AY 17.

3.3. Effect of initial pH solution

pH of the dye solution for the removal process influences not only the surface charge of the nano-agents and the dissociation of functional groups of the active sites on its surface, but also the aqueous chemistry of the dye.

As shown in Fig. 6, the effects of initial solution pH on the AY 17 removal by Fe^0 NPs, PO, PO-IPA, PO-CHA, Fe^0-PO-IPA and Fe^0-PO-CHA were investigated. The main reason of decreasing the dye removal by Fe^0 NPs at the low pHs can be due to the following reactions. Fe^{2+} can be the major redox active ion in this system as iron corrosion in anoxic and or oxic environments by the reactions [58],

$$Fe^0 + 2H_2O \rightarrow Fe^{2+} + H_2 + 2OH^-$$

$$2Fe^0 + O_2 + 2H_2O \rightarrow 2Fe^{2+} + 4OH^-$$

Significant increases in pH accompany both reactions. Following the initial reaction, and increase of pH, released ferrous iron will precipitate as $Fe(OH)_2$ due to its low solubility ($K_{sp} = 8.0 \times 10^{-16}$ at 25 °C).

The more consumption of Fe^0 NPs, in absence of the dissolved oxygen with purging purified N_2, due to reacting OH^- (in the reactions) with H^+ (in the solution) at low pHs causes that the less Fe^0 NPs react with the dye, so its removal through the cleavage of azo bond is reduced.

As seen for other agents, the dye removal decreased with increasing pH. It shows that –COOH and –OH groups in PO, PO-IPA, PO-CHA, Fe^0-PO-IPA and Fe^0-PO-CHA could be the main responsible of the AY 17 removal by adsorption according to the pointed reason in Section 3.2.

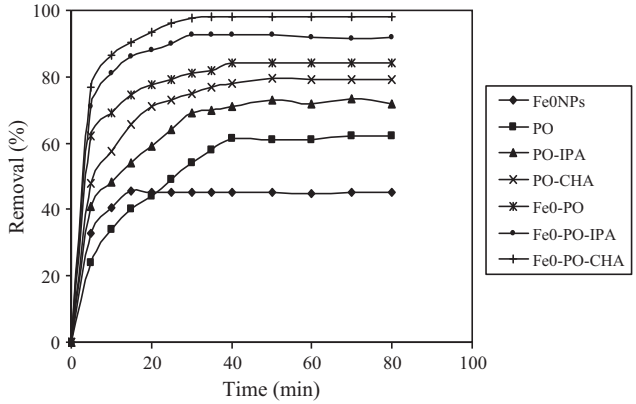

Fig. 7. Effect of contact time on the AY 17 removal by the kinds of remover agents. Initial solution pH: for Fe^0 NPs 6.0 ± 0.1 and for others 3.0 ± 0.1, initial concentration of AY 17: 200 ppm, remover agents dose: 2.0 g/L, temperatures: 298 K, agitation rate: 300 rpm.

3.4. Effect of contact time

Fig. 7 suggests that the removal of AY 17 by Fe^0-PO-CHA and Fe^0-PO-IPA has both the highest kinetic and capacity, so that at the first 30–35 min it is nearly completed and the removal percent of the dye was obtained 92.8 and 97.8, respectively, for the dye initial concentration of 200 ppm, at the pointed optimum conditions in the caption of Fig. 7.

The contact time of 100 min was selected in this study to complete the equilibrium, viz the optimum values of AY 17 removal were obtained after nearly that time. The initial high removal rate of AY 17 within the first 10–40 min was attributed to the high availability of binding sites on the surface of nanoparticles, and the subsequent lower sorption rate decreased the availability of binding sites on the surface of nanoparticles after 40 min due to the removal of the initial AY 17 molecules.

The arrangement of the kinetic of the agents is observed as:
PO < Fe^0 NPs < PO-IPA < PO-CHA < Fe^0-PO-IPA < Fe^0-PO-CHA
while the arrangement of the dye capacity of the agents are as:
Fe^0 NPs < PO < PO-IPA < PO-CHA < Fe^0-PO-IPA < Fe^0-PO-CHA

3.5. Effect of temperature

As shown in Fig. 8, raising the temperature has a positive impact on the AY removal for all of the agents. The removal efficiency reaction increased from about 33% to 55% for Fe^0 NPs, 53% to 66% for

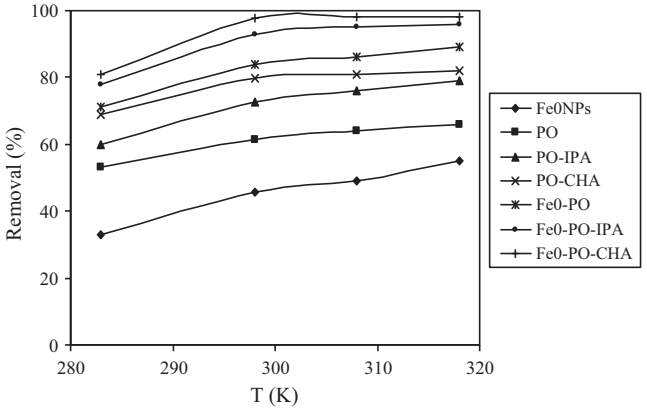

Fig. 8. Effect of temperature on the AY 17 removal by the kinds of remover agents. Initial solution pH: for Fe^0 NPs 6.0 ± 0.1 and for others 3.0 ± 0.1, initial concentration of AY 17: 200 ppm, remover agents dose: 2.0 g/L, contact time: 100 min, agitation rate: 300 rpm.

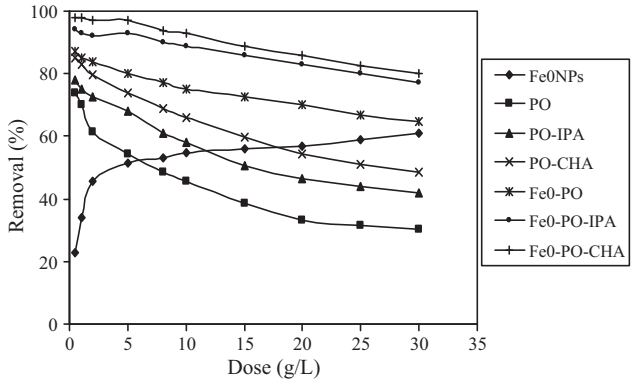

Fig. 9. Effect of remover agents dose on the AY 17 removal by the kinds of remover agents. Initial solution pH: for Fe^0 NPs 6.0 ± 0.1 and for others 3.0 ± 0.1, initial concentration of AY 17: 200 ppm, contact time: 100 min, temperatures: 298 K, agitation rate: 300 rpm.

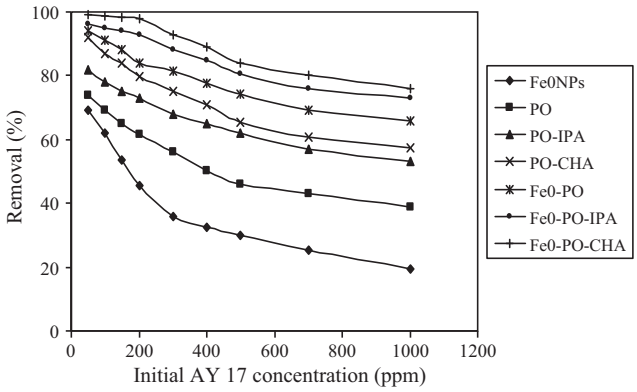

Fig. 10. Effect of initial concentration of AY 17 on its removal by the kinds of remover agents. Initial solution pH: for Fe^0 NPs 6.0 ± 0.1 and for others 3.0 ± 0.1, remover agents dose: 2.0 g/L, contact time: 100 min, temperatures: 298 K, agitation rate: 300 rpm.

extracted pectin, 60% to 79% for PO-IPA 69% to 82% for PO-CHA, 78% to 96% for Fe^0-PO-IPA and 81% to 98% for Fe^0-PO-CHA as the result of the temperature increase from 10 to 45 °C, for the dye initial concentration of 200 ppm, at the pointed optimum conditions in the caption of Fig. 8. It is obviously proved that higher reaction temperature can reduce the time required for AY removal.

3.6. Effect of dosage, and the rule of adsorption and reduction processes

This study was done for the agents of the dye removal with the dosages of 0.5–30.0 g/L at the shown parameters (see Fig. 9). As seen, the removal percent of AY 17 increased with increasing dosage when Fe^0 NPs was only used. It increased from 23.1% to 61.5% when the dosage of Fe^0 NPs was increased from 0.5 to 30.0 g/L. It could be due to increasing the reactive sites of Fe^0 NPs which remove the dye molecules through reduction, generally, viz. an electron transfer process. Therefore, crowding Fe^0 NPs due to increasing the dosage, in spite of the agglomeration of these nanoparticles, not only did not reduce the dye removal but also increased it, remarkably, whereas for other agents the removal percent of AY 17 decreased with increasing the dosages.

The reason of decreasing the dye removal with increasing other agent dosages could be due to decreasing the active surface area of pectin structure as the main factor of the dye removal by overlapping or aggregation during the sorption. Because, the dye adsorption by functional groups of the stabilizers viz. pectin and its cross linking agents is performed through a mass transfer process and crowding these large polymer structures could be an inhibitor factor.

As seen in Fig. 9, the decreasing rate of the AY 17 removal for Fe^0-PO-IPA and Fe^0-PO-CHA was less than that, when the extracted pectin, PO-IPA and PO-CHA were used. It could be due to the joint role of reduction by Fe^0- and adsorption by -PO-IPA and -PO-CHA in the structure of these agents.

In other words, the dosage change of Fe^0- (nano structure) had a reverse effect on the dye removal as compared with the dosage change effect of -PO-IPA and -PO-CHA (polymer structure) on the removal. On the other hand, decreasing the removal can show that the adsorption process of the dye by the polymer structure was more effective than the reduction process by the nano structure of Fe^0-.

3.7. Effect of AY initial concentration

As seen from Fig. 10, the removal percent decreased with increasing the initial concentration (C_o) of AY 17 for all the agents. The decrease of the removal percent by each agent was due to increasing the amount of the removed dye. Also, the more decrease of the removal percent by each agent in comparison with other, due to the same increasing the initial concentration, shows the less increase of the removal amount.

For instance, decreasing the removal percent from 69% (for C_o = 50 ppm) to 30% (for C_o = 500 ppm) by Fe^0 NPs was due to increasing the removed amount from 34.5 to 150 ppm, respectively, viz. increasing 115.5 ppm in the removed amount, whereas decreasing the removal percent from 74% to 46% for the mentioned initial concentration by the extracted pectin was due to increasing the removed amount from 37 to 230 ppm, respectively, viz. increasing 193 ppm in the removed amount.

In other words, the rate of decreasing the removal percent by Fe^0 NPs up to the first 500 ppm was more than that, when were used other agents. It showed that the dependency of the dye removal percent on the initial concentration by Fe^0 NPs in the first initial concentrations, especially, was more than that of others. It shows that Fe^0 NPs had the least rate, and Fe^0-PO-IPA and Fe^0-PO-CHA had the most rate of increasing the removed amount.

It could be due to both the agglomeration of Fe^0 NPs and having no the stabilizer polymer structure and its adsorption mechanism, in comparison with Fe^0-PO-IPA and Fe^0-PO-CHA.

4. Conclusions

On the basis of the experimental results of this investigation, the following conclusions can be drawn:

1. The TEM images show that the diameter of Fe^0 NPs was not less than 10 nm and about 80% of them were between 30 and 45 nm. About 3% of these particles were about 50 nm in diameter, whereas the stabilized particles by stabilizers as discrete particles were not more than 45 nm.
2. The separation of the symmetric and asymmetric stretches of the carboxylate group was 175 cm^{-1} for Fe^0-PO-CHA and 207 cm^{-1} for Fe^0-PO-IPA in FT-IR spectra, so bidentate bridging and monodentate interaction could be the primary mechanisms for binding PO-CHA and PO-IPA molecules to Fe^0 NPs, respectively.
3. The results of XRD image indicate that the modification of Fe^0 NPs by pectin and cross-linked ones have not changed the crystal structure of nanoparticles. But the intensity of the peaks corresponding to surface functional groups is reduced by using pectin and cross-linking agents. This reduction for Fe^0-PO-CHA is more than Fe^0-PO-IPA.

4. The dye removal by Fe^0 NPs decreased at the low pHs. Because, Fe^0 can be converted to Fe^{2+} and OH^- is produced that H^+ at the low pHs with using hydroxyl ion consume Fe^0.
5. The removal of AY 17 by biopolymer structures in PO, PO-IPA, PO-CHA, Fe^0–PO, Fe^0-PO-IPA and Fe^0-PO-CHA decreased with increasing pH. Because, –COOH and –OH groups as the main responsible of the AY 17 removal by adsorption are converted to $–COOH_2^+$ and $–OH_2^+$ at the acidic pHs, so an electrostatic attraction is happened between these positive groups and $–SO_3^-$ of the acidic dye.
6. The reason of increasing AY 17 removal with increasing the dosage of Fe^0 NPs could be due to increasing the reactive sites of Fe^0 NPs which remove the dye molecules through reduction, generally, viz. an electron transfer process. Therefore, crowding Fe^0 NPs due to increasing the dosage, in spite of the agglomeration of these nanoparticles did not reduce the dye removal.
7. The dye adsorption by functional groups of the stabilizers viz. pectin and its crosslinking agents is performed through a mass transfer process and crowding these large polymer structures could be an inhibitor factor.

Acknowledgments

The authors are grateful to the Islamic Azad University, Mrs. M. Ebadi and Dr. Sina from Tehran University for their help and support.

References

[1] O. Ligrini, E. Oliveros, A. Braun, Photochemical processes for water treatment, Chem. Rev. 93 (1993) 671–698.
[2] J.M. Wang, C.P. Huang, H.E. Allen, D.K. Cha, D.W. Kim, Adsorption characteristics of dye onto sludge particulates, J. Colloid Interface Sci. 208 (1998) 518–528.
[3] S.Y. Oh, D.K. Cha, P.C. Chiu, B.J. Kim, Conceptual comparison of pink water treatment technologies: granular activated carbon anaerobic fluidized bed, and zero-valent iron-Fenton process, Water Sci. 49 (2004) 129–136.
[4] T. Zhou, Y.Z. Li, F.S. Wong, X.H. Lu, Enhanced degradation of 2,4-dichlorophenol by ultrasound in a new Fenton like system (Fe/EDTA) at ambient circumstance, Ultrason. Sonochem. 15 (2008) 782–790.
[5] A. Mittal, G. Vibha, J. Mittal, Removal and recovery of hazardous triphenylmethane dye, methyl violet through adsorption over granulated waste materials, J. Hazard. Mater. 150 (2008) 364–375.
[6] A. Mittal, D. Kaur, J. Mittal, Batch and bulk removal of a triarylmethane dye, Fast Green FCF, from wastewater by adsorption over waste materials, J. Hazard. Mater. 163 (2009) 568–577.
[7] A. Mittal, J. Mittal, A. Malviya, V.K. Gupta, Adsorptive removal of hazardous anionic dye Congo red from wastewater using waste materials and recovery by desorption, J. Colloid Interface Sci. 340 (1) (2009) 16–26.
[8] A. Mittal, D. Kaur, A. Malviya, J. Mittal, V.K. Gupta, Adsorption studies on the removal of coloring agent phenol red from wastewater using waste materials as adsorbents, J. Colloid Interface Sci. 337 (2) (2009) 345–354.
[9] V.K. Gupta, A. Mittal, A. Malviya, J. Mittal, Adsorption of carmoisine A from wastewater using waste materials – bottom ash and de-oiled soya, J. Colloid Interface Sci. 335 (1) (2009) 24–33.
[10] A. Mittal, J. Mittal, A. Malviya, V.K. Gupta, Removal and recovery of Chrysoidine Y from aqueous solutions by waste materials, J. Colloid Interface Sci. 344 (2) (2010) 497–507.
[11] A. Mittal, V.K. Gupta, A. Malviya, J. Mittal, Process development for the batch and bulk removal and recovery of a hazardous, water-soluble azo dye (Metanil Yellow) by adsorption over waste materials (Bottom Ash and De-Oiled Soya), J. Hazard. Mater. 151 (2008) 821–832.
[12] A. Mittal, J. Mittal, L. kurup, A.K. Singh, Process development for the removal and recovery of hazardous dye erythrosine from wastewater by waste materials—Bottom Ash and De-Oiled Soya as adsorbents, J. Hazard. Mater. 138 (2006) 95–105.
[13] A. Mittal, D. Kaur, J. Mittal, Applicability of waste materials—bottom ash and deoiled soya—as adsorbents for the removal and recovery of a hazardous dye, brilliant green, J. Colloid Interface Sci. 326 (2008) 8–17.
[14] A. Mittal, J. Mittal, A. Malviya, D. Kaur, V.K. Gupta, Decoloration treatment of a hazardous triarylmethane dye, Light Green SF (Yellowish) by waste material adsorbents, J. Colloid Interface Sci. 342 (2010) 518–527.
[15] A. Mittal, R. Jain, J. Mittal, S. Varshney, S. Sikarwar, Removal of Yellow ME 7 GL from industrial effluent using electrochemical and adsorption techniques, Int. J. Environ. Pollut. 43 (4) (2010) 308–323.
[16] A. Mittal, Use of hen feathers as potential adsorbent for the removal of a hazardous dye, J. Hazard. Mater. 128 (2006) 233–239.
[17] J.R. Perey, P.C. Chiu, C.P. Huang, D.K. Cha, Zero-valent iron pretreatment for enhancing the biodegradability of azo dyes, Water Environ. Res. 74 (2002) 221–225.
[18] S.J. Allen, G. Mckay, J.F. Porter, Adsorption isotherm models for basic dye adsorption by peat in single and binary component systems, Colloid Int. Sci. 280 (2004) 322–333.
[19] G. Mckay, M. El-guendi, M.M. Nassar, Adsorption model for the removal of acid dyes from effluent by bagasse pith using a simplified isotherm, Adsorpt. Sci. Technol. 15 (1997) 251–270.
[20] G. Mckay, V.J.P. Poots, Kinetics and diffusion process in colour removal from effluent using wood as an adsorbent, J. Chem. Biotechnol. 30 (1980) 279–292.
[21] M. Rachakornkij, Removal of dyes using bagasse fly ash, J. Sci. Technol. 26 (2004) 14–20.
[22] Y. Fu, T. Viraraghavan, Column studies for biosorption of dye from aqueous solutions on immobilised *Aspergillus niger* fungal biomass, Water Sci. 29 (2003) 465–472.
[23] S. Schiewer, S.B. Patil, Pectin-rich fruit wastes as biosorbents for heavy metal removal: equilibrium and kinetics, Bioresour. Technol. 99 (2008) 1896–1903.
[24] T. Padmesh, K. Vijayaraghavan, G. Sekaran, M. Velan, Batch and column studies on biosorption of acid dyes on fresh water macro alga *Azolla filiculoides*, J. Hazard. Mater. B125 (2005) 121–129.
[25] R. Zhang, X. Wang, One step synthesis of multiwalled carbon nanotube/gold nanocomposites for enhancing electrochemical response, Chem. Mater. 19 (2007) 976–978.
[26] S. Ikeda, Y. Ikoma, H. Kobayashi, T. Harada, T. Torimoto, B. Ohtanic, M. Matsumura, Encapsulation of titanium(IV) oxide particles in hollow silica for size-selective photocatalytic reactions, Chem. Commun. 36 (2007) 3753–3755.
[27] T. Gao, Q. Li, T. Wang, Sonochemical synthesis, optical properties, and electrical properties of core/shell-type ZnO nanorod/CdS nanoparticle composites, Chem. Mater. 17 (2005) 887–892.
[28] J.T. Nurmi, P.G. Tratnyek, V. Sarathy, D.R. Baer, J.E. Amonette, K. Pecher, C. Wang, J.C. Linehan, D.W. Matson, R.L. Penn, M.D. Driessen, Characterization and properties of metallic iron nanoparticles: spectroscopy, electrochemistry, and kinetics, Environ. Sci. Technol. 39 (2005) 1221–1230.
[29] J. Fan, Y. Guo, J. Wang, M. Fan, Rapid decolorization of azo dye methyl orange in aqueous solution by nanoscale zerovalent iron particles, J. Hazard. Mater. 166 (2009) 904–910.
[30] M. Hou, F. Li, X. Liu, X. Wang, H. Wan, The effect of substituent groups on the reductive degradation of azo dyes by zerovalant iron, J. Hazard. Mater. 145 (2007) 305–314.
[31] Y. Liu, G.V. Lowry, Effect of particle age (Fe^0 content) and solution pH on NZVI reactivity: H_2 evolution and TCE dechlorination, Environ. Sci. Technol. 40 (2006) 6085–6090.
[32] B.A. Manning, J.R. Kiser, H. Kwon, S.R. Kanel, Spectroscopic investigation of Cr(III)- and Cr(VI)-treated nanoscale zerovalent iron, Environ. Sci. Technol. 41 (2007) 586–592.
[33] G.C.C. Yang, H.L. Lee, Chemical reduction of nitrate by nanosized iron: kinetics and pathways, Water Res. 39 (2005) 884–894.
[34] B.L. Cushing, V.L. Kolesnichenko, C.J. O'Connor, Recent advances in the liquid-phase syntheses of inorganic nanoparticles, Chem. Rev. 104 (2004) 3893–3946.
[35] S. Sun, H. Zeng, Size-controlled synthesis of magnetite nanoparticles, J. Am. Chem. Soc. 124 (2002) 8204–8205.
[36] D.K. Kim, M. Mikhaylova, Y. Zhang, M. Muhammed, Protective coating of superparamagnetic iron oxide nanoparticles, Chem. Mater. 15 (2003) 1617–1625.
[37] H. Khalil, D. Mahajan, M. Rafailovich, M. Gelfer, K. Pandya, Synthesis of zerovalent nanophase metal particles stabilized with poly- (ethylene glycol), Langmuir 20 (2004) 6896–6903.
[38] Q. Wang, H. Qian, Y. Yang, Z. Zhang, C. Naman, X. Xu, Reduction of hexavalent chromium by carboxymethyl cellulose-stabilized zero-valent iron nanoparticles, J. Contam. Hydrol. 114 (2010) 35–42.
[39] S.M. Ponder, J.G. Darab, J. Bucher, D. Caulder, I. Craig, L. Davis, N. Edelstein, W. Lukens, H. Nitsche, L. Rao, D.K. Shuh, T.E. Mallouk, Surface chemistry and electrochemistry of supported zerovalent iron nanoparticles in the remediation of aqueous metal contaminants, Chem. Mater. 13 (2001) 479–486.
[40] F. He, D. Zhao, J. Liu, C.B. Roberts, Stabilization of Fe–Pd nanoparticles with sodium carboxymethyl cellulose for enhanced transport and dechlorination of trichloroethylene in soil and groundwater, Ind. Eng. Chem. Res. 46 (2007) 29–34.
[41] N. Saleh, T. Phenrat, K. Sirk, B. Dufour, J. Ok, T. Sarbu, K. Matyjaszewski, R.D. Tilton, G.V. Lowry, Adsorbed triblock copolymers deliver reactive iron nanoparticles to the oil/water interface, Nano Lett. 5 (2005) 2489–2494.
[42] A. Jauneau, M. Quentin, A. Driouich, Micro-heterogeneitly of pectins and calcium distribution in the epidermal and cortical *parenchyma* cell wall of flax hypocotyls, Protoplasma 189 (1997) 9–19.
[43] A. Synytsya, J. Copikova, P. Matejka, V. Mackovic, Fourier transform Raman and infarared spectroscopy of pectins, Carbohydr. Polym. 54 (2003) 97–106.
[44] F. Ting Li, H. Yang, Y. Zhao, R. Xu, Novel modified pectin for heavy metal adsorption, Chin. Chem. Lett. 18 (2007) 325–328.
[45] K. Vijayaraghavan, J. Mao, Y.S. Yun, Biosorption of methylene blue from aqueous solution using free and polysulfone-immobilized *Corynebacterium glutamicum*: batch and column studies, Bioresour. Technol. 99 (2008) 2864–2871.
[46] F. Colak, N. Atar, A. Olgun, Biosorption of acidic dyes from aqueous solution by *Paenibacillus macerans*: kinetic, thermodynamic and equilibrium studies, Chem. Eng. J. 150 (2009) 122–130.

[47] R. Rakhshaee, M. Giahi, A. Pourahmad, Studying effect of cell wall's carboxyl–carboxylate ratio change of *Lemna minor* to remove heavy metals from aqueous solution, J. Hazard. Mater. 163 (2009) 165–173.
[48] M. Masmoudi, S. Besbes, M. Chaabouni, C. Robert, Optimization of pectin extraction from lemon by-product with acidified date juice using response surface methodology, Carbohydr. Polym. 74 (2008) 185–192.
[49] R. Rakhshaeea, M. Panahandeh, Stabilization of a magnetic nano-adsorbent by extracted pectin to remove methylene blue from aqueous solution: a comparative studying between two kinds of cross-likened pectin, J. Hazard. Mater. 189 (2011) 158–166.
[50] G.B. Deacon, R.J. Phillips, Relationship between the carbon-oxygen stretching frequencies of carboxylate complexes and the type of carboxylate coordination, Coord. Chem. Rev. 33 (1980) 227–250.
[51] N. Wu, L. Fu, M. Su, M. Aslam, K.C. Wong, V.P. Dravid, Interaction of fatty acid monolayers with cobalt nanoparticles, Nano Lett. 4 (2004) 383–386.
[52] Y.T. Lin, C.H. Weng, F.Y. Chen, Effective removal of AB24 dye by nano/micro-size zero-valent iron, Sep. Purif. Technol. 64 (2008) 26–30.
[53] K. Sohn, S.W. Kang, S. Ahn, M. Woo, S.K. Yang, Fe(0) nanoparticles for nitrate reduction: stability, reactivity, and transformation, Environ. Sci. Technol. 40 (2006) 5514–5519.
[54] Y.H. Liou, S.L. Lo, C.J. Lin, W.H. Kuan, S.C. Weng, Chemical reduction of an unbuffered nitrate solution using catalyzed and uncatalyzed nanoscale iron particles, J. Hazard. Mater. 127 (2005) 102–110.
[55] X. Li, D.W. Elliott, W. Zhang, Zero-valent iron nanoparticles for abatement of environmental pollutants: materials and engineering aspects, Crit. Rev. Solid State Mater. Sci. 31 (2006) 111–122.
[56] J.A. Mielczarski, G.M. Atenas, E. Mielczarski, Role of iron surface oxidation layers in decomposition of azo-dye water pollutants in weak acidic solutions, Appl. Catal. B. Environ. 56 (2005) 289–303.
[57] J. Bandara, J.A. Mielczarski, J. Kiwi, Molecular mechanism of surface recognition. Azo dyes degradation on Fe, Ti, and Al oxides through metal sulfonate complexes, Langmuir 15 (1999) 7670–7679.
[58] Y. Furukawa, J.W. Kim, J. Watkins, R.T. Wilkin, Formation of ferrihydrite and associated iron corrosion products in permeable reactive barriers of zero-valent iron, Environ. Sci. Technol. 36 (2002) 5469–5475.